The wing surface pressure distribution with leading-edge correction included is

$$C_p = 1 - Q^2/U^2 \tag{29}$$

where Q/U is given in Eq. (28).

Acknowledgments

This research was supported by NASA Langley Research Center under Grant NCC1-41. The author wishes to thank Dr. John Lamar of NASA for his help and interest throughout the course of the research.

References

[1] Jones, R. T., "Properties of Low-Aspect-Ratio Pointed Wings at Speeds Below and Above the Speed of Sound," NACA Rept. 835, 1946.

[2] Levin, D. and Seginer, A., "Chordwise and Compressibility Correction for Arbitrary Planform Slender Wings," *AIAA Journal*, Vol. 20, Aug. 1982, pp. 1025-1030.

[3] Wang, K. C., "A New Approach to 'Not-so-Slender' Wing Theory," *Journal of Mathematics and Physics*, Vol. XLVII, No. 4, Dec. 1968, pp. 391-406.

[4] Weber, J., "The Calculation of the Pressure Distribution on Thick Wings of Small Aspect Ratio at Zero Lift in Subsonic Flow," Aeronautical Research Council, R&M 2993, Sept. 1954.

[5] Cheng, H. K. and Rott, N., "Generalizations of the Inversion Formula of Thin Airfoil Theory," *Journal of Rational Mechanics and Analysis*, Vol. 3, No. 3, May 1954, pp. 357-382.

[6] Kulfan, R. M., "Wing Airfoil Shape Effects on the Development of Leading-Edge Vortices," AIAA Paper 79-1675, 1979.

[7] Van Dyke, M. D., "Subsonic Edges in Thin-Wing and Slender-Body Theory," NACA TN 3343, 1954.

Cellular Patterns in Poststall Flow over Unswept Wings

D. Weihs* and J. Katz†
Technion – Israel Institute of Technology
Haifa, Israel

Introduction

THE growing fleet of general aviation aircraft has focused increased attention on the poststall aerodynamics of unswept wings, with the purpose of improving the stall/spin resistant characteristics of these airplanes. Flow visualization experiments[1-7] with such wings indicated that beyond stall the nature of the separated flow is strongly three-dimensional, even when very high-aspect-ratio wing planforms were tested. Under those conditions the oil flow patterns on the upper surface of the wings appeared to be cellular in shape, similar to the one shown in Fig. 1. Furthermore, it was observed that when the wing aspect ratio is increased the number of cells grows, with limited variation in the "natural size" of these cells.[6]

No theoretical interpretation exists for the prediction of the nature of this complex three-dimensional flow. Therefore, this Note proposes a mechanism for the production of such cells based on an analysis of the stability of the separation vortices. This enables an approximate calculation of the large-scale geometry of the separation cells.

Received June 24, 1982; revision received Nov. 30, 1982.

*Professor, Department of Aeronautical Engineering.

†Senior Lecturer, Department of Mechanical Engineering. Member AIAA.

The Flow Model

As a result of increasing the angle of attack of the high-aspect-ratio unswept wing up to the fully stalled flow condition, a separation line will initially progress forward on the wing upper surface. The location of this line will be prescribed by the wing camber, angle of attack, and Reynolds number. Along this separation line a shear flow regime exists that constantly generates vorticity, as shown in Fig. 2a. This vorticity is aggregated to form a "time average/vortex core" that pulsates both in location and strength to generate the well-known von Kármán street vortex pattern observed in the two-dimensional cross section.[8-10] However, the pure two-dimensional (or straight) vortex core of Fig. 2a is not stable and a wavy disturbance will develop (Fig. 2b), resulting in the three-dimensional time-averaged vortex pattern proposed in Fig. 2c. Surface oil flow visualization conforming to this model will result in formations as shown by Fig. 2d, which are similar to those reported in many experiments (Refs. 1-7 and Fig. 1).

To study the production of the cellular spanwise structure of the separated wake, we return to the case of Fig. 2a and specifically to the vortex above the upper surface of the wing (Fig. 3). As mentioned above, it is assumed that the configuration of Fig. 2a is the time-averaged configuration, with further vorticity buildup being periodically shed into the wake. Thus, we have the quasi-two-dimensional situation of Fig. 3 where the vortex core is located such that the relative velocity between point "a" and the wing is zero. The profile serves approximately as a reflecting plane for the vortex, i.e., resulting in an equivalent image vortex. Assuming the upper surface of the wing to be approximately flat in the region

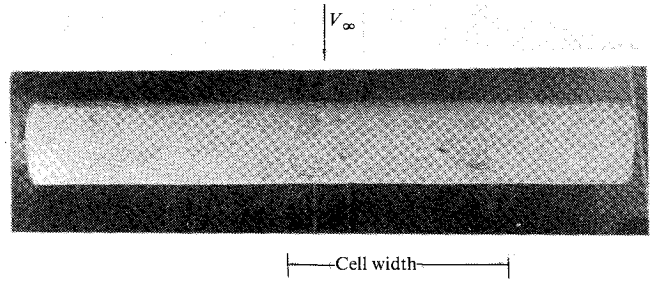

Fig. 1 Oil flow patterns on the upper surface of a stalled wing (NACA 0012 airfoil at $\alpha = 14$ deg, $\mathcal{R} = 7$, $Re = 0.2 \times 10^5$).

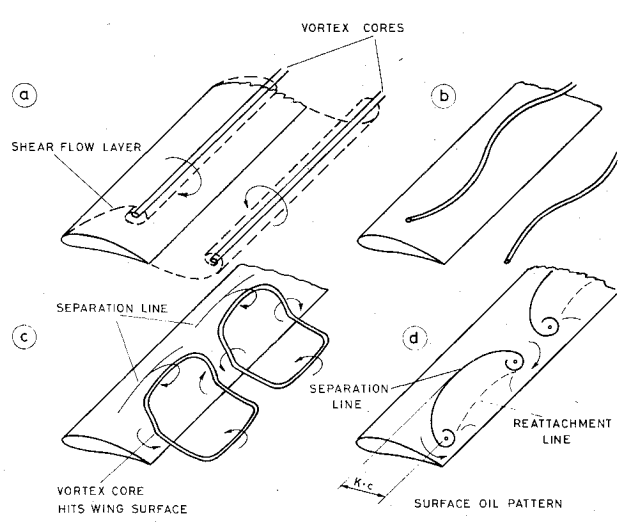

Fig. 2 Schematic of the vortex instability and the resulting cellular shapes in the separated flow over rectangular wings.

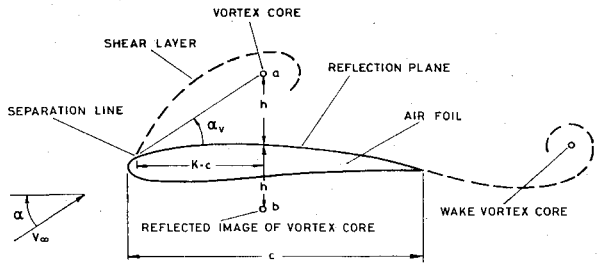

Fig. 3 Vortex model geometry.

directly underneath the separation bubble, we can take the image vortex to be at point "b" of Fig. 3. The flow along the lower surface will probably not be adequately described by this model, but this is not directly relevant to the present problem.

The wake vortex sheet will usually be much further from the separation vortex, and essentially we have one pair of equal strength counterrotating line vortices. Such a pair, when immersed in oncoming flow, provide a steady flow pattern reminiscent of the far wake of a finite wing. In the latter case, the oncoming flow is caused by the downwash component that results in the vortex pair moving down. This configuration is steady, but unstable, and tends to break up into sections by means of a symmetrical mode of longitudinal waves as shown by Crow.[11]

We propose here that the spanwise cells observed may be the result of such a Crow-type instability in the spanwise direction. This instability when amplified will develop a wavy deformation of the vortex line located at point "a" of Fig. 3; consequently, similar deformations will be induced on the wake vortex as proposed in Fig. 2b. The pair of counterrotating line vortices at points "a" and "b" of Fig. 3 are thus subject to a symmetric wavy instability causing typical wavelengths 8.6 times[11] the undisturbed distance between the vortices.

The distance h can be found from the relation (see Fig. 3)

$$h = K c \tan\alpha_v \tag{1}$$

where c is the chord, α_v the angle between the chord line and the line connecting the separation line and the vortex center, and K the fraction of the chord at which the vortex is centered. K and α_v are empirical constants still to be established. From Crow's analysis,

$$\lambda/2h \cong 8.6 \tag{2}$$

Defining the cell length (in the spanwise direction) as λ and the span as b we can now relate the number of cells n to the aspect ratio by

$$b/c = n\lambda/c \tag{3}$$

Substituting Eq. (1) into Eq. (3) we obtain

$$n = b/17.2Kc\tan\alpha_v \tag{4}$$

and for a rectangular wing, the aspect ratio is $\mathcal{R} = b/c$ and

$$n = \mathcal{R}/17.2K\tan\alpha_v \tag{5}$$

where the value of K and α_v still have to be established.

When the perturbations caused by the instability start growing, the sections of the vortex line deflected from the original position are also moved in the chordwise direction, with the portions moving closer to the wing being moved upstream as a result of the enhanced induced velocity due to the image vortex (see Fig. 2b). Thus, the traces left by oil flow visualizations on the wing surface are expected to be the projection of the lower part of the sinusoidal wavy vortex lines. This is an approximation, as we tacitly assume the vortex shapes to be unchanged as the deflections grow out of the linear range. However, observation of such oil traces (Fig. 1 and Winkelmann[2-6]) shows these predictions are fulfilled. This approach also enables a rough estimate of the parameter K in Eqs. (1) and (5) from flow visualization data.

Since both the separation line and the vortex core line are clearly shown by oil surface visualization (as defined in Fig. 2d), it is assumed that their chordwise dislocation equals $K \cdot c$. Furthermore, if α_v is approximated to be the angle of attack for which the flow separation is first observed,[5] then from the data presented by Winkelmann and Barlow[3] it is found that K is between 0.3 and 0.5, and $\alpha_v = 18.4$ deg. Substituting these values into Eq. (5) with $K = 0.4$ we obtain

$$n = \mathcal{R}/2.28 \tag{6}$$

The wing planforms are of finite span so that this analysis has to take into account the tip effect, that can be seen as a forcing function for the instability. Thus, a whole number of wavelengths (cells) is expected, this number being the closest integer from below to n of Eq. (6). The predicted number of cells by Eq. (6) for the wings shown in Ref. 3 are one for the wing having $\mathcal{R} = 1$, two for $\mathcal{R} = 6$, three for $\mathcal{R} = 9$, and five for $\mathcal{R} = 12$. Similar agreement between the predicted and observed number of cells is found by observing Fig. 1 where $K \sim 0.6$ and $\mathcal{R} = 7, \alpha_v = 14$ deg (the early separation here is a result of the low Reynolds number $= 0.2 \times 10^4$). By substituting these values into Eq. (5), the value of $n = 2.72$ is obtained, indicating the existence of the two cells present in Fig. 1.

Once the above cellular pattern has been developed, a further increase in the wing angle of attack will result in an expansion of the wavelength of each cell until their boundaries unify. However, after this initial cell formation, their number remained constant and a change in their number with additional increases in the angle of attack were not observed.

Conclusions

The model presented here proposes a first-order estimate for calculating the relation between a rectangular wing aspect ratio and the number of cellular shapes appearing in the separated flow. The derived relation is based on the quasisteady instability of two infinite parallel vortex lines and the predicted and observed number of those cellular shapes are in good agreement. However, further investigation is required to determine the development of the wavy disturbance proposed in this Note and the dynamic formation of these vortex rings and their overall time-dependent nature.

References

[1] Moss, G. F. and Murdin, P. M., "Two Dimensional Low-Speed Tunnel Tests on the N.A.C.A. 0012 Section Including Measurements Made During Pitching Oscillation at the Stall," Royal Aeronautical Establishment, TR 68104, May 1968.

[2] Winkelmann, A. E., Barlow, J. B., Saini, J. K., Anderson, J. D. Jr., and Jones, E., "The Effect of Leading Edge Modifications on the Post Stall Characteristics of Wings," AIAA Paper 80-0199, 1980.

[3] Winkelmann, A. E. and Barlow, J. B., "Flow Field Model for a Rectangular Planform Wing beyond Stall," *AIAA Journal,* Vol. 18, Aug. 1980, pp. 1006-1008.

[4] Meznarsic, V. F. and Gross, L. W., "An Experimental Investigation of a Wing with Controlled Mid-Span Flow Separation," AIAA Paper 80-1804, 1980.

[5] Winkelmann, A. E. and Tsao, C. P., "An Experimental Study of the Flow on a Wing with Partial Span Drooped Leading Edge," AIAA Paper 81-1665, Aug. 1981.

[6] Winkelmann, A. E., "An Experimental Study of Separated Flow on a Finite Wing," AIAA Paper 81-1882, Aug. 1981.

[7] Bippes, H., Jacob, K., and Turk, M., "Experimental Investigation of the Separated Flow Around a Rectangular Wing," DFVLR, Gottingen, FRG, DFVLR-Forschungsbericht 81-12, 1981 (in German).

[8]Katz, J., "A Discrete Vortex Method for the Unsteady Separated Flow over an Airfoil," *Journal of Fluid Mechanics,* Vol. 102, 1981, pp. 315-328.
[9]Fage, A. and Johansen, F. C., "On the Flow of Air Behind an Inclined Flat Plate of Infinite Span," *Proceedings of the Royal Society of London,* Series A, Vol. 116, 1927, pp. 170-197.
[10]McAlister, K. W. and Carr, L. W., "Water Tunnel Experiments on an Oscillating Airfoil at $R_e = 21{,}000$," NASA TN-2502.
[11]Crow, S. C., "Stability Theory for a Pair of Trailing Vortices," *AIAA Journal,* Vol. 8, Dec. 1970, pp. 2172-2177.

Accuracy of Approximations to the Navier-Stokes Equations

J. D. Murphy*
NASA Ames Research Center, Moffett Field, California

Introduction

TO avoid the complexity and the large computational costs of solutions to the full Navier-Stokes equations, systems of truncated differential equations have been proposed[1-3] which offer advantages in computational efficiency while capturing all the physically relevant behavior. The hierarchy of these systems is: the classical boundary-layer equations with specified edge properties (usually the streamwise pressure distribution), the coupled boundary-layer/inviscid equations, the so-called thin-layer equations which discard streamwise diffusion, and the Navier-Stokes equations.

In the present Note, we consider each of these approximations applied to an incompressible, laminar-separating flow at low and moderate Reynolds numbers.

Analysis

If we restrict our attention to two-dimensional, incompressible steady laminar flow, the entire hierarchy can be represented by the nondimensional equations

$$\omega = \frac{\partial^2 \psi}{\partial y^2} + \frac{K_1}{R_E}\frac{\partial^2 \psi}{\partial x^2}$$

$$\frac{\partial \psi}{\partial y}\frac{\partial \omega}{\partial x} - \frac{\partial \psi}{\partial x}\frac{\partial \omega}{\partial y} = \frac{\partial^2 \omega}{\partial y^2} + \frac{K_2}{R_E}\frac{\partial^2 \omega}{\partial x^2} \qquad (1)$$

where ψ is the dimensionless stream function and ω is the dimensionless vorticity. (For definitions of the transformation variables see Ref. 4.)

A particular member of the above hierarchy can be obtained by the appropriate choice of K_1 and K_2, as shown in Table 1.

Using a slightly modified version of the computer code of Ref. 4 applied to Eq. (1) we can treat each of these levels of approximation *within a single logical and numerical framework so that differences between solutions can be attributed to the equations solved and not to the method of solution.* We apply this code to a strongly retarded flow, at two Reynolds numbers, $UL/\nu = 9{,}000$ and 900,000. For discussion purposes, approximations (2) and (3) in Table 1 will be termed higher approximations.

Received Aug. 2, 1982; revision received Feb. 16, 1983. This paper has been declared a work of the U. S. Government and therefore is in the public domain.
*Research Scientist.

Results and Discussion

In the present case, the low Reynolds number problem for the strongly retarded flow corresponds to Briley's case 4,[5] the high Reynolds number case has the same boundary conditions but the viscosity has been reduced by a factor of 10^2. Comparisons of the results obtained using the methods of Refs. 4 and 5 are considered in Ref. 4. Figure 1 shows the freestream velocity distribution, imposed at the outer computational boundary for this case.

Figure 2 shows the nondimensional skin friction vs distance along the plate for a strongly retarded flow. The higher approximations do very well and the principal higher-order effect is the interaction between the viscous and inviscid flows. Each of the higher approximations can compute through the separation point without difficulty. Although the coupled boundary-layer/inviscid calculation differs most from the full equations, it is still quite satisfactory despite a very low Reynolds number.

To determine the effect of Reynolds number, the same case was rerun at a Reynolds number 100 times larger. In Fig. 3, the results for the strongly retarded flow at high Reynolds number are presented, and again the higher approximations are indistinguishable from the solutions to the full equations.

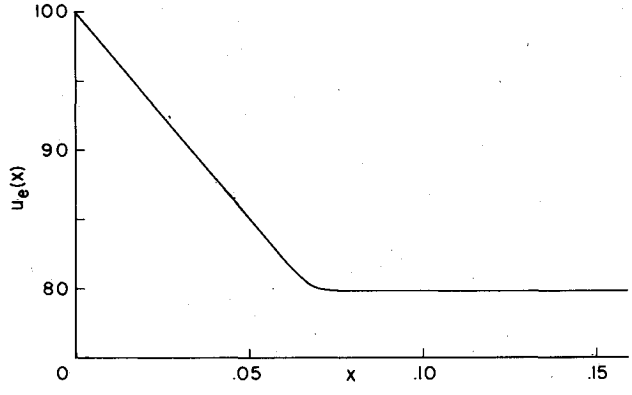

Fig. 1 Freestream velocity distribution.

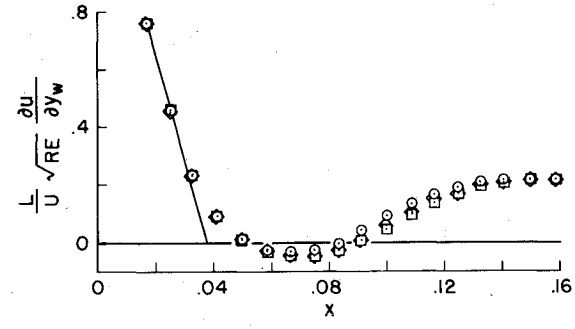

Fig. 2 Comparison of dimensionless wall shear stress in low Reynolds number strongly retarded flow.

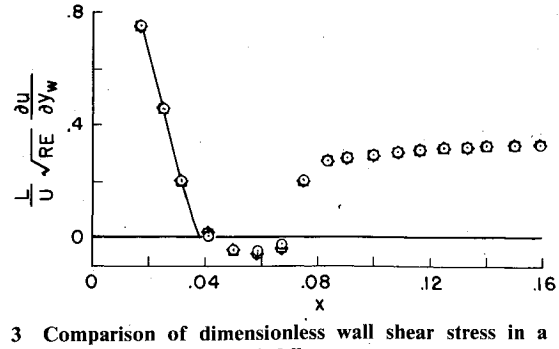

Fig. 3 Comparison of dimensionless wall shear stress in a high Reynolds number strongly retarded flow.